Broadband time-resolved elliptical crystal spectrometer for X-ray spectroscopic measurements in laser-produced plasmas*

Wang Rui-Rong(王瑞荣)†, Jia Guo(贾 果), Fang Zhi-Heng(方智恒),
Wang Wei(王 伟), Meng Xiang-Fu(孟祥富), Xie Zhi-Yong(谢志勇), and Zhang Fan(张 帆)

Shanghai Institute of Laser Plasma, Shanghai 201800, *China*

(Received 15 January 2014; revised manuscript received 16 April 2014; published online 17 September 2014)

The X-ray spectrometer used in high-energy-density plasma experiments generally requires both broad X-ray energy coverage and high temporal, spatial, and spectral resolutions for overcoming the difficulties imposed by the X-ray background, debris, and mechanical shocks. By using an elliptical crystal together with a streak camera, we resolve this issue at the SG-II laser facility. The carefully designed elliptical crystal has a broad spectral coverage with high resolution, strong rejection of the diffuse and/or fluorescent background radiation, and negligible source broadening for extended sources. The spectra that are Bragg reflected ($23^\circ < \theta < 38^\circ$) from the crystal are focused onto a streak camera slit 18 mm long and about 80 μm wide, to obtain a time-resolved spectrum. With experimental measurements, we demonstrate that the quartz(1011) elliptical analyzer at the SG-II laser facility has a single-shot spectral range of (4.64–6.45) keV, a typical spectral resolution of $E/\Delta E = 560$, and an enhanced focusing power in the spectral dimension. For titanium (Ti) data, the lines of interest show a distribution as a function of time and the temporal variations of the He-α and Li-like Ti satellite lines and their spatial profiles show intensity peak red shifts. The spectrometer sensitivity is illustrated with a temporal resolution of better than 25 ps, which satisfies the near-term requirements of high-energy-density physics experiments.

Keywords: X-ray spectrum, red shift, time-dependent phenomena

PACS: 32.30.Rj, 32.70.Jz, 31.70.Hq **DOI:** 10.1088/1674-1056/23/11/113201

1. Introduction

X-ray spectroscopy is a well established diagnostic technique for high-energy-density physics experiments, including the direct-drive scheme of inertial confinement fusion (ICF).[1,2] X-ray emissions from highly charged H-, He-, Li-, Be-, and Ne-like ions are traditionally chosen to obtain information on multi-charged ion spectra.[3,4] New X-ray spectroscopic techniques allow us to obtain more accurately the wavelengths of the X-ray spectral lines and the ionization potentials of the multi-charged ions by using a traditional plasma source. It is now also possible to observe (and to identify) new lines of emission (such as dielectron satellites to resonance transitions in H-, He-, and Ne-like ions and radiative transitions from the Rydberg states of the multi-charged ions). An analysis of the spectrally and temporally resolved X-ray emission from a laser-produced plasma has demonstrated that it is a powerful method for diagnosing plasma parameters and determining the spatial structure.[5–8] The spectroscopic investigation of high-temperature laser-produced plasmas and high-energy-density physics experiments require both broad X-ray energy coverage and high spectral, spatial, and temporal resolutions.[9,10] A streak camera is typically used in these applications.[11] The traditional spectroscopic diagnostic instruments typically employ flat crystal spectrometers[12] equipped with streak cameras. The flat crystals are usually positioned at ∼(10–50) mm from the target, and the streak camera is used to record the temporal variation of the plasma emissions. The main drawback of the traditional spectroscopic diagnostic system is that the crystal located close to the target inevitably receives some damage. One possible solution is to use bent crystals. In this paper, we design an X-ray spectroscopic diagnostic system by carefully choosing a crystal with an elliptical geometry. The X-ray source is located at one focus of the ellipse, then the X-ray emissions reflected by the crystal are converged to the other focus, where a slit 18 mm long and approximately 80 μm wide is located. The slit is used to shield the detector from unwanted radiation. A streak camera is positioned behind the slit to record the spectrum. The X-rays reflected by the crystal are focused onto the streak camera to obtain a time-resolved spectrum. The concave curvature of the elliptical surface reduces source broadening, which is the apparent energy spread at the detector plane caused by the finite size of the monochromatic source. Therefore the focusing power in the spectral dimension is enhanced. Then the elliptical bent design offers a spectral resolution comparable to flat crystals, while achieving a greater spectral range.

In this paper, we present the broadband time-resolved elliptical crystal spectrometer installed at the Shenguang-II (SG-II) laser facility. The spectrometer, which was constructed for high-resolution studies of the emissions from laser-produced plasmas, can be used for obtaining broadband, temporal, and spectral resolved spectra. This paper is organized as follows.

*Project supported by the National Natural Science Foundation of China (Grant No. 11175167).
†Corresponding author. E-mail: wangrr59@sina.com

In Section 2, we briefly introduce the experimental setup, and then the experimental results are presented and analyzed. Finally, discussion and conclusions are presented.

2. Diagnostic configuration

In this paper, the SG-II laser facility is used to produce high-energy-density thermal plasmas. The broadband time-resolved elliptical crystal spectrometer is installed on the SG-II laser facility. The X-ray spectroscopy diagnostic system consists of an elliptically blend crystal, an alignment telescope, and an X-ray streak camera. Figure 1 shows the details of the experimental setup. X-rays that satisfy the Bragg condition are reflected into the X-ray streak camera. Better time resolution and high spectral resolution have been considered when designing this diagnostic system. The streak camera elliptical analyzer X-ray spectrograph will be referred to as the SEAXS system in the following.

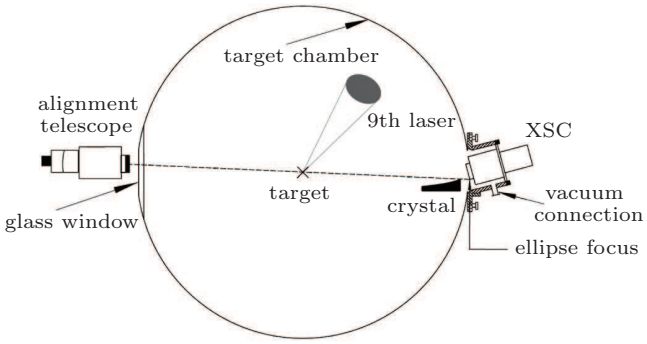

Fig. 1. Diagram of the spectrometers as they are fielded in the experiment at the SG-II laser facility.

It is immediately evident that the SEAXS system allows a large spectral range to be measured and a large working distance to the source. The elliptical analyzer has an 860 mm focal length. X-rays Bragg reflected ($23^\circ < \theta < 38^\circ$) from the crystal are focused through the other focal point. The important advantages of the elliptical analyzer include not only that its crossover point is fixed for all Bragg reflections, but also that its crossover is real as established at the focal point for the given elliptical geometry. With the elliptical analyzer, an effective scatter aperture can be located at the crossover position. This feature is also important because only a small diffracting region of the analyzer can be seen at the associated point on the detection, thus the effect of the diffuse and/or fluorescent background radiation from the total illuminated surface of the analyzer can be reduced.

The SEAXS system has been used on plane targets irradiated by a frequency-doubled laser ($\lambda = 527$ nm) extracted from the SG-II Nd:glass laser system. The laser pulse bandwidth was about 1 ns. The laser focus condition was set to 150 μm in diameter. For all experiments, the total laser energy on the plane target was about 1.2 kJ. The target materials were chosen to produce K-shell and L-shell emission lines in the spectral ranges of the crystals. An example of the initial tests of the X-ray streak camera (a photograph recorded spectra using a 100 μm Be foil across the scatter aperture, quartz(1011) analyzing crystal, and CsI transmission photocathode) is shown in Fig. 2.

3. Experimental results

Figure 2 shows a digitized spectral image captured by the SEAXS system. The spectral lines are measured using the quartz analyzer for highly ionized species of titanium (Ti). The horizontal axis is the spectral dimension, and the vertical axis shows the time. It can be seen from Fig. 2 that the spectra exhibit isolated peaks. The small spectral widths of the observed lines make it possible to measure the wavelengths with a very good accuracy. This provides detailed spectra comparable to the flat-crystal survey spectrometer,[12] but also with temporal resolution. As time goes on, the intensity peak moves to lower energy and then decreases gradually; such an energy spectral line bend and the shape of the given feature are obvious. The time evolution of these emission lines is measured in a temporal window of about 800 ps. In Fig. 2, a data file of optical intensity versus position is given. The detector position is converted to the photon energy using the reference lines as the standards for wavelength calibration to avoid the uncertainties. The wavelengths of the reference lines are taken from Ref. [13]. The absolute accuracy of our wavelength measurements is defined mainly by the accuracy of the reference lines and is better than 0.2 mÅ for the reference lines. A data processing package is used to analyze the precision of the spectral wavelength calibration. The experimental error of the average wavelength is within ±0.002 Å.

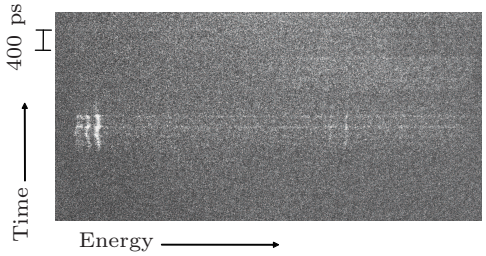

Fig. 2. Photograph of the X-ray streak camera output for a spectrum presented to a CsI transmission photocathode by a quartz elliptical analyzer. Measured Ti K-shell X-ray time-resolved spectrum from the Ti foil.

Figure 3 shows the spectra obtained with the SEAXS system. The 2P→1S lines, inner-shell transition lines we observed, are primarily from helium and lithium-like ions. The Ti Kβ, Ly-α, and Ly-β lines appear weak. The full widths at half maximum (FWHMs) of several energy spectral lines are independently measured to determine the spectral resolving power $E/\Delta E_{\mathrm{FWHM}}$. A typically measured resolution of $E/\Delta E$ (energy spectral line band ΔE) is approximately 560 in the energy spectral range 4.64 keV$< E <$ 6.45 keV, which is in good

agreement with our design goal. Calculations of the temporal resolution of the camera based on the streak velocity, the spatial resolution of the streak tube and intensifier, the entrance slit widths, and the photoelectron energy spread from the photocathode show that the resolution should be better than 25 ps. Note the good line-to-background contrast ratio; this enabled us to study in detail the line profiles and the line-to-continuum ratios. The electron temperature of the laser-induced coronal plasma can be deduced from the intensity ratios of various lines and also from the intensity ratios of such lines and the continuum.

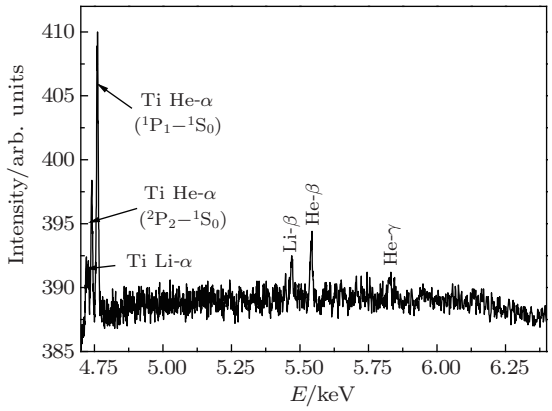

Fig. 3. Time-integrated titanium X-ray spectral image.

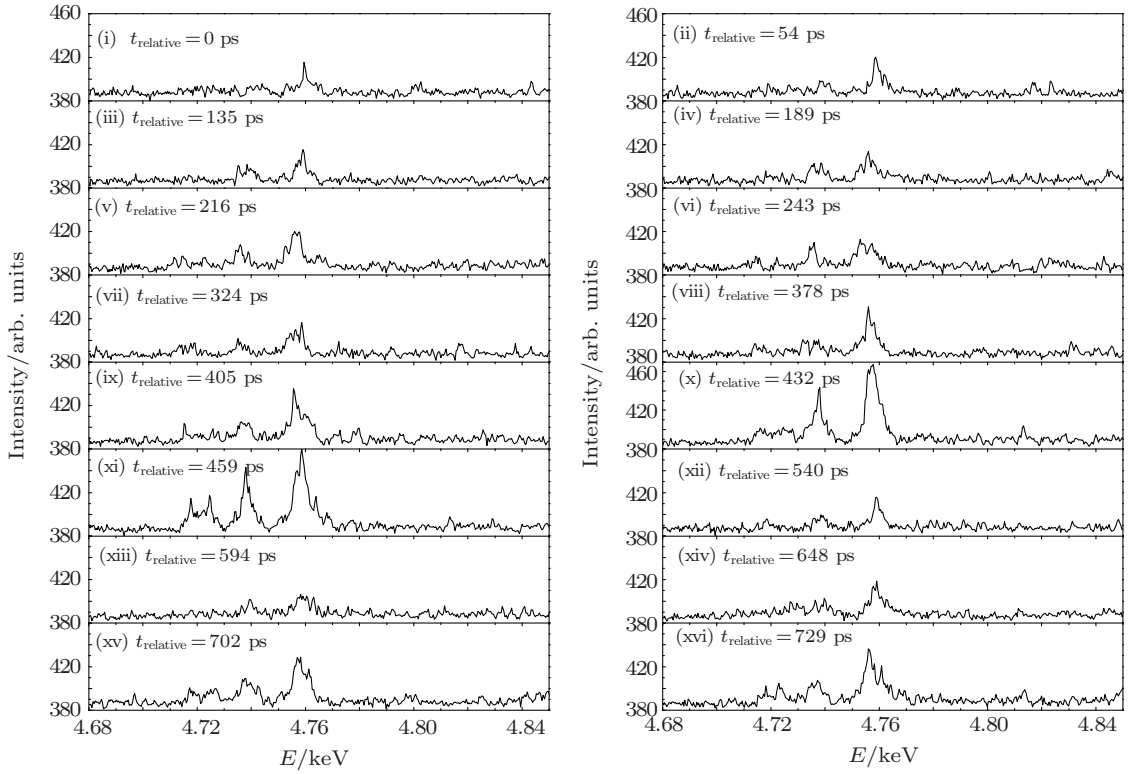

Fig. 4. Temporal variations of the spectra shown in Fig. 2 for 16 different times.

A time-integrated X-ray image of the Ti He-α and Li-like satellite lines is shown in Fig. 3, and the spectral shapes at 16 different times are shown in Fig. 4. Because the emission from the Ly-β line is too weak to be used in analysis, we focus on the He-α and Li-like satellite lines. The starting time ($t = 0$) in the E–t diagram is arbitrarily chosen. The intensity of the Ti He-α line increases continuously until $t_{\text{relative}} = 459$ ps and then decreases. The intensity peak of the Ti He-α line moves to lower energy. The typical shift velocity is 3.5 eV/54 ps as seen in Fig. 5. The red shift of the Ti He-α line begins to decrease until it disappears after the red shift peak phase. The mechanisms include the following. The first is the Doppler shift due to the movement of the hot high-density region away from the XSC. The second is the displacement of the emission source in a plane of dispersion of the spectrometer. The displacement can be determined by the geometrical configuration of the XSC. The third is that the emission of the Li-like satellite lines, particularly $1s^2 3l$–$1s3p3l$, becomes strong. These satellites are due to the excitation of the states having a spectator electron at the level of $n = 3$ (n is the principal quantum number). This means that the populations of the doubly excited states (1s3l3p) are larger than those of the singly excited states (1s3p). The doubly excited states are mainly populated due to the recombination processes, such as the electron impact (three-body) recombination[14] and/or the radiative recombination. The rate coefficients for both recombination pro-

cesses become larger when the electron temperature decreases or the electron density increases. In Fig. 3, the Li-like satellite line in the energy spectral range of interest is also visible. This is important as it excludes the contributions of the Li-like satellite lines on the low-energy wing of the He-α line. The fourth and the only plausible interpretation for the energy shift is the plasma density effect.[15,16] Laser-created plasmas can be a way to reach a state of strongly coupled matter, i.e. where the Coulomb energy between ions is much higher than their kinetic energy. Under these conditions, the atomic properties of the ions change: atomic orbitals overlap and are deformed, producing in particular a modification of the external energy levels and of the characteristic highly ionized spectrum. Under these circumstances, the He-α and Li-like satellite lines can show shift and broadening in energy. A more detailed and quantitative analysis for these atomic processes in the plasma is necessary in a future work.

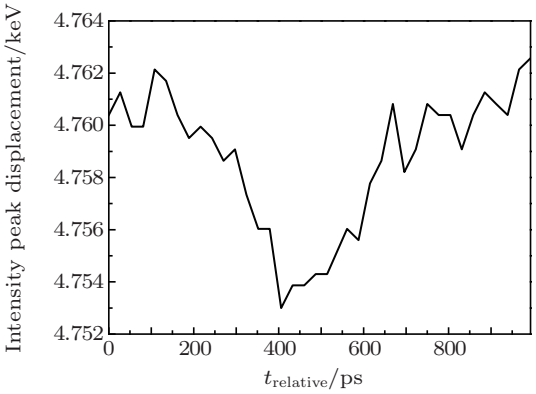

Fig. 5. Temporal variation of the He-α ($^1P_1$–$^1S_0$) emission intensity peak displacement.

4. Discussion and conclusion

A broadband high-resolution SEAXS system has been designed to measure laser-induced X-ray spectra. Temporal variations of Ti K-shell emissions of Ti He-α, He-β, He-γ, Li-α, and Li-β were measured with the SEAXS system, and their spectral line profiles were also shown as a function of time. The evolution of these emission lines was measured in a temporal window of about 800 ps. The experimental results showed that the SEAXS system has a typically measured resolution of $E/\Delta E = 560$ and a temporal resolution better than 25 ps over the Bragg reflected angle range of 23°–38°. In addition, the spectral lines exhibited a slight curvature that is probably due to the red shift of the intensity peak. A more detailed and quantitative analysis is needed to improve the atomic physics model, including, for example, ladder-like transitions. The broadband high-resolution SEAXS system has been fielded at the SG-II laser facility. The spectral range and resolution and the temporal resolution are suitable for planned high-energy-density physics experiments on various lasers.

The instrument may be improved in the future by evolving in response to the need for higher data quality, greater flexibility, and better time and spectral resolutions. In particular, the SEAXS system built should ensure continuous coverage of spectral ranges important to specific experiments. This will enable the estimation of the temperature and the density of the laser-produced plasma in a more convincing manner.

Acknowledgements

The authors sincerely acknowledge Prof. Xiao Sha-Li from Chongqing University for his fruitful suggestions on this study. This work could not be done without the collaboration of the experimental crew in laser operation, target fabrication, and plasma measurements. All their efforts are gratefully appreciated.

References

[1] Yaakobi B, Steel D, Thorsos E, Hauer A and Perry B 1977 *Phys. Rev. Lett.* **39** 1526
[2] Haynes D A, Hooper Jr C F, Mancini Jr R C, Bradley D K, Delettrez J, Epstein R and Jaanimagi P A 1995 *Rev. Sci. Instrum.* **66** 755
[3] Szlachetko M, Berset M, Dousse J C, Hoszowska J and Szlachetko J 2013 *Rev. Sci. Instrum.* **84** 093104
[4] Hammel B A, Keane C J, Kania D R, Kilkenny J D, Lee R W, Pasha R and Turner R E 1992 *Rev. Sci. Instrum.* **63** 5017
[5] Bordner E S, Colombant D G, Gardner J H, Lehinberg R H, Obenschain S P, Phillips L, Schmitt A J, Stthian J D, McCrory R L, Seka W, Verdon C P, Knauer J P, Afeyan B B and Powell H T 1998 *Phys. Plasmas* **5** 1901
[6] Anderson S G, Heeter R F, Booth R, Emig J, Fulkerson S, McCarvile T, Norman D and Young K F 2006 *Rev. Sci. Instrum.* **77** 063115
[7] Bailey J E, Chandler G A, Slutz S A, Golovkin I, Lake P W, MacFarlane J J, Mancini R C, Burris-Mog T J, Cooper G, Leeper R L, Mehlhlhorn T A, Moore T C, Nash T J, Nielsen D S, Ruiz C L, Schroen D G and Varnum W A 2004 *Phys. Rev. Lett.* **92** 085002
[8] Zeng J L, Zhao G and Yuan J M 2005 *Chin. Phys. Lett.* **22** 1972
[9] Heeter R F, Anderson S G, Booth R, Brown G V, Eming J, Fulkerson S, McCarville T, Norman D, SchneiderMB and Young B K F 2008 *Rev. Sci. Instrum.* **79** 10E303
[10] Lake P W, Bailey J E, Rochau G A, Moore T C, Petmecky D P and Gard P 2004 *Rev. Sci. Instrum.* **75** 3690
[11] McCarville T, Fulkerson S, Booth R, Eming J, Young B, Anderson S and Heeter B 2005 *Rev. Sci. Instrum.* **76** 103501
[12] Wang R R, Chen W M, Mao C S, Dong J Q and Fu S Z 2009 *Chin. Opt. Lett.* **7** 156 (in Chinese)
[13] Wang R R, Chen W M, Wang W, Dong J Q and Xiao S L 2010 *Chin. Phys. B* **19** 075202
[14] Salzmann D and Krumbein A 1978 *J. Appl. Phys.* **49** 3229
[15] Koening M, Malnoult P and Nguyen H 1988 *Phys. Rev. A* **38** 2089
[16] Wu Z Q, Han G X and Pang J Q 2002 *Chin. Phys. Lett.* **19** 518